THE JOURNAL OF COMPARATIVE NEUROLOGY 284:275–293 (1989)

Axon-Bearing Amacrine Cells of the Macaque Monkey Retina

DENNIS M. DACEY
Department of Biological Structure, The University of Washington, Seattle, Washington 98195

ABSTRACT

A new and remarkable type of amacrine cell has been identified in the primate retina. Application of the vital dye acridine orange to macaque retinas maintained in vitro produced a stable fluorescence in the somata of apparently all retinal neurons in both the inner nuclear and ganglion cell layers. Large somata (~15–20 μm diam) were also consistently observed in the approximate center of the inner plexiform layer (IPL). Intracellular injections of horseradish peroxidase (HRP) made under direct microscopic control showed that the cells in the middle of the IPL constitute a single, morphologically distinct amacrine cell subpopulation. An unusual and characteristic feature of this cell type is the presence of multiple axons that arise from the dendritic tree and project beyond it to form a second, morphologically distinct arborization within the IPL; these cells have thus been referred to as axon-bearing amacrine cells.

The dendritic tree of the axon-bearing amacrine cell is highly branched (~40–50 terminal dendrites) and broadly stratified, spanning the central 50% of the IPL so that the soma is situated between the outermost and innermost branches. Dendritic field size increases from ~200 μm in diameter within 2 mm of the fovea to ~500 μm in the retinal periphery. HRP injections of groups of neighboring cells revealed a regular intercell spacing (~200–300 μm in the retinal periphery), suggesting that dendritic territories uniformly cover the retina.

One to four axons originate from the proximal dendrites as thin (<0.5 μm), smooth processes. The axons increase in diameter (~1–2 μm) as they course beyond the dendritic field and bifurcate once or twice into secondary branches. These branches give rise to a number of thin, bouton-bearing collaterals that extend radially from the dendritic tree for 1–3 mm without much further branching. The result is a sparsely branched and widely spreading axonal tree that concentrically surrounds the smaller, more highly branched dendritic tree. The axonal tree is narrowly stratified over the central 10–20% of the IPL; it is approximately ten times the diameter of the dendritic tree, resulting in a 100 times greater coverage factor.

The clear division of an amacrine cell's processes into distinct dendritic and axonal components has recently been observed in other, morphologically distinct amacrine cell types of the cat and monkey retina and therefore represents a property common to a number of functionally distinct cell types. It is hypothesized that the axon-bearing amacrine cells, like classical neurons, use action potentials to transmit signals over long distances in the IPL and, on the basis of previous immunohistochemical results, contain the inhibitory neurotransmitter GABA.

Key words: primate, retinal amacrine cells, in vitro, horseradish peroxidase, intracellular staining

Accepted January 26, 1989.

The amacrine cells of the vertebrate retina are a major class of interneurons that make synaptic contact exclusively in the inner plexiform layer (IPL) where they influence the transmission of signals from the bipolar cells to the ganglion cells, the output neurons of the retina. The amacrine cells are surely the most diverse and least understood population of vertebrate retinal neurons, and it has long been recognized that this cell class must compose a large number of functionally distinct subpopulations. As a group they show a great variety of shapes and dendritic field sizes (e.g., Kolb et al., '81, '88), contain a number of neuroactive peptides and virtually every classical neurotransmitter candidate (reviews: Brecha, '83; Dowling, '87), may be both pre- and postsynaptic to bipolar cells, ganglion cells, and to each other (Dowling and Boycott, '66; Dowling, '68; Sakai et al., '86), and may give rise to only graded potential changes or to spikelike impulses (Miller and Dacheux, '76; Barnes and Werblin, '86; review: Miller, '79).

Recently the discovery of markers for specific cell types has made it possible to identify clearly and characterize the morphology of distinct amacrine cell types. The advantage of this approach is that an entire subpopulation of cells may be revealed for analysis. For example, the fluorescent molecule 4,6-diamidino-2-phenylindole (DAPI) has been used as a marker for the cholinergic amacrine cell population in rabbit retina (Tauchi and Masland, '84) and for a morphologically identified glycine-accumulating amacrine cell (the AII amacrine) in the cat's retina (Vaney, '85). Other fluorescent markers have been used to identify and study possible serotoninergic (Vaney, '86; Sandell and Masland, '86; Wässle et al., '87) and dopaminergic amacrine cell populations (Tauchi and Masland, '86; Voigt and Wässle, '87; Dacey, '88, '89). In each of these studies it was possible to determine from the numbers and unique shape of a given cell type the density and spatial arrangement of the dendritic plexus that arises from the total population of identified cells. This is a particularly significant step in developing hypotheses for the function of morphologically distinct cell types because of the possibility that individual amacrine cell processes establish electrically and synaptically isolated components (e.g., Elias and Stevens, '80; Miller and Bloomfield, '83; Masland et al., '84).

In this paper a new amacrine cell type in the macaque retina is identified and characterized with the light microscope following intracellular HRP injections. The cell type was observed in an in vitro whole-mount preparation after staining with the fluorescent vital dye acridine orange. Acridine orange is nonselective, brightly labeling the somata of apparently all retinal neurons; however, one population of cells was selectively identified by their large size and unusual but consistent location in the approximate center of the IPL. These unique features permitted the cells to be targeted for intracellular staining under direct microscopic control. The most striking feature of this cell type is the presence of multiple axons that arise from and project for millimeters beyond the dendritic tree, suggesting that the axon-bearing amacrine cells may use spiking axons to convey signals laterally within the IPL.

MATERIALS AND METHODS

In vitro preparation

Retinas were obtained from the tissue program of the Regional Primate Research Center at the University of Washington. A total of 18 retinas were obtained from *Macaca nemestrina* (n = 4) and *M. fascicularis* (n = 14). The animal was placed under deep barbiturate anaesthesia and the eyes were removed. Each eye was immediately hemisected and the vitreous was removed. The eyecup was placed in oxygenated Ames medium (Ames and Nesbett, '81), and the retina was dissected, care being taken to remove any remaining vitreous from the retinal surface. A series of radial cuts were made in the retina, and it was laid flat, vitreal-side up, in a superfusion chamber and mounted on the stage of a light microscope equipped for episcopic illumination. The bottom of the chamber is formed by a microscope slide and the retina is held in place by adherence to a thin layer of gelatin on the slide. The retinas were viewed with either transmitted or episcopic illumination while being continuously superfused with oxygenated Ames medium (~3 ml/minute). Retinal cells were stained in vitro by adding a few drops of acridine orange (~1 mM solution in Ames medium) to the chamber while continuing the superfusion to wash away excess dye. Retinas were maintained in vitro for several hours at room temperature with no apparent deterioration in cellular morphology at the light microscopic level.

Intracellular injections of HRP and Lucifer Yellow

Intracellular microelectrodes were formed from thin-walled microcapillary glass pulled to an initial resistance of 175–250 MΩ on a Brown-Flaming micropipette puller. The electrodes were filled with a 4% solution of rhodamine-conjugated HRP (Sigma) and Lucifer Yellow (Aldrich) in MOPS buffer (pH 7.6) and beveled to a final resistance of 70–100 MΩ with a K.T. Brown beveler. The epifluorescence microscope used to observe the in vitro fluorescence is equipped with a stage-mounted micromanipulator such that microelectrodes can be positioned independently of focus (stage height). An oil-driven microdrive mounted to the manipulator was used to advance the microelectrode manually. The electrode tip and the retina were viewed together at high resolution with a 40× water-immersion, long-working-distance objective (Zeiss) that was modified to permit the proper angle of electrode approach to the tissue (Brown and Flaming, '86).

Both Lucifer Yellow fluorescence in the microcapillary electrode and the acridine fluorescence can be observed with the same filter combination (excitation filter, 410–490 nm; barrier filter 515 nm long pass). This permitted the electrode tip to be positioned near the fluorescing cell under direct microscopic control. Cell penetration was achieved by tapping the base of the microscope and subsequently confirmed while still observing the target cell by passing Lucifer Yellow into the cell with negative current (0.1–1.0 namp for 5–10 seconds). If the penetration was successful, the cell was then injected with rhodamine-HRP by passing positive current (3–8 namps; 1–3 minutes). The accumulation of rhodamine-HRP in the cell and the quality of the cell's morphology were directly monitored by observing the rhodamine fluorescence (excitation filter, 545 nm; barrier filter, 590 nm) slowly increase in brightness and extend into the cell's processes during the course of the injection. Retinas were removed from the superfusion chamber after 2–5 hours and fixed in phosphate-buffered 1% glutaraldehyde (0.1 M; pH 7.4) for 2 hours. HRP reaction product was demonstrated in the intact retinal whole mounts by using diaminobenzidine as the chromagen according to a standard proto-

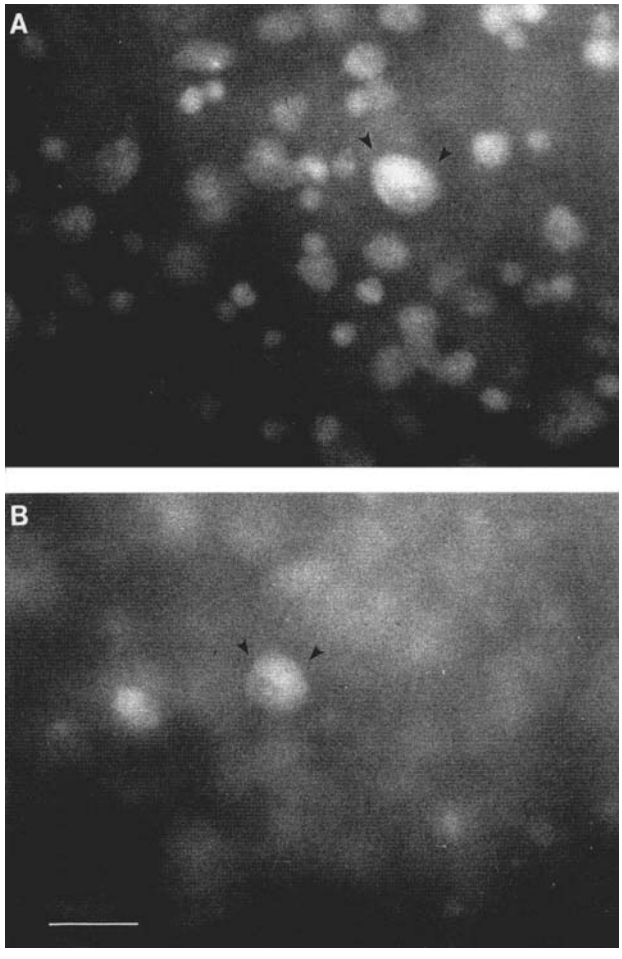

Fig. 1. Acridine orange fluorescence in a whole-mount in vitro preparation of *Macaca fascicularis* retina. **A:** Plane of focus in the ganglion cell layer shows a range of soma sizes and shapes that accumulate the dye and fluoresce green under blue episcopic illumination. The large soma of a parasol ganglion cell is indicated by the arrowheads. **B:** Plane of focus shifted to the approximate center of the inner plexiform layer (IPL) illustrates a single, weakly fluorescent soma (arrowheads). Cells of this size, shape, and unusual laminar position were consistently observed with acridine fluorescence in vitro. Intracellular HRP injections into these cells showed that they constitute a single amacrine cell type whose distinct morphology is detailed in the following figures. Excitation filter, 410–490 nm; barrier filter, 515 long pass. Scale bar = 50 μm.

col (Dacey, '85). The retinas were mounted on slides vitreal-side up without counterstaining.

Data analysis

Soma and dendritic field sizes were determined for a sample of 64 HRP injected cells that appeared to show complete filling. The reaction product within these cells appeared uniformly dark out to the distal dendritic tips. Cells judged to be incompletely filled showed lighter and nonuniform filling marked by gradual fading of the HRP reaction product in the distal dendrites. Soma area was determined by entering the soma outline (at 1,500×) into a computer via a graphics tablet. Soma diameter was expressed as the diameter of a circle with the same area. To calculate dendritic field area a convex polygon was traced around the dendritic field perimeter (at 400×) and entered into a computer via a graphics tablet. Dendritic field diameter was expressed as the diameter of a circle with the same area as that of the polygon.

For 58 cells the stratification of the dendritic tree and soma within the IPL was determined from the whole mounts by reading the scale on the microscope focus knob (calibrated to 1 μm intervals). For each cell a depth reading was taken for the borders of the inner nuclear and ganglion

Fig. 2. Figure 2 appears on pages 279–281. Illustration of the distinct dendritic tree and axonal tree of the axon-bearing amacrine coll of the IPL. **A:** Low-magnification photo-micrograph of a single, HRP-filled cell shows the dendritic tree in the center surrounded by long, sparsely branching processes. Scale bar = 200 μm. **B:** Complete camera lucida tracing of a second cell reveals this pattern more clearly and shows that the long processes all originate from the dendritic tree of the injected cell. Scale bar = 400 μm. **C:** Higher magnification of the dendritic tree and the proximal parts of the axons of the cell shown in B. Thick proximal dendrites give rise to multiple axons that extend beyond the dendritic tree where they begin to branch. The origin of four axons is indicated by the arrowheads. **D:** Higher magnification of part of the axonal arborization of the cell shown in B. Thick parent axons (arrows) give rise to long collateral branches that bear distinct varicosities along their lengths. Scale bar in C and D = 100 μm.

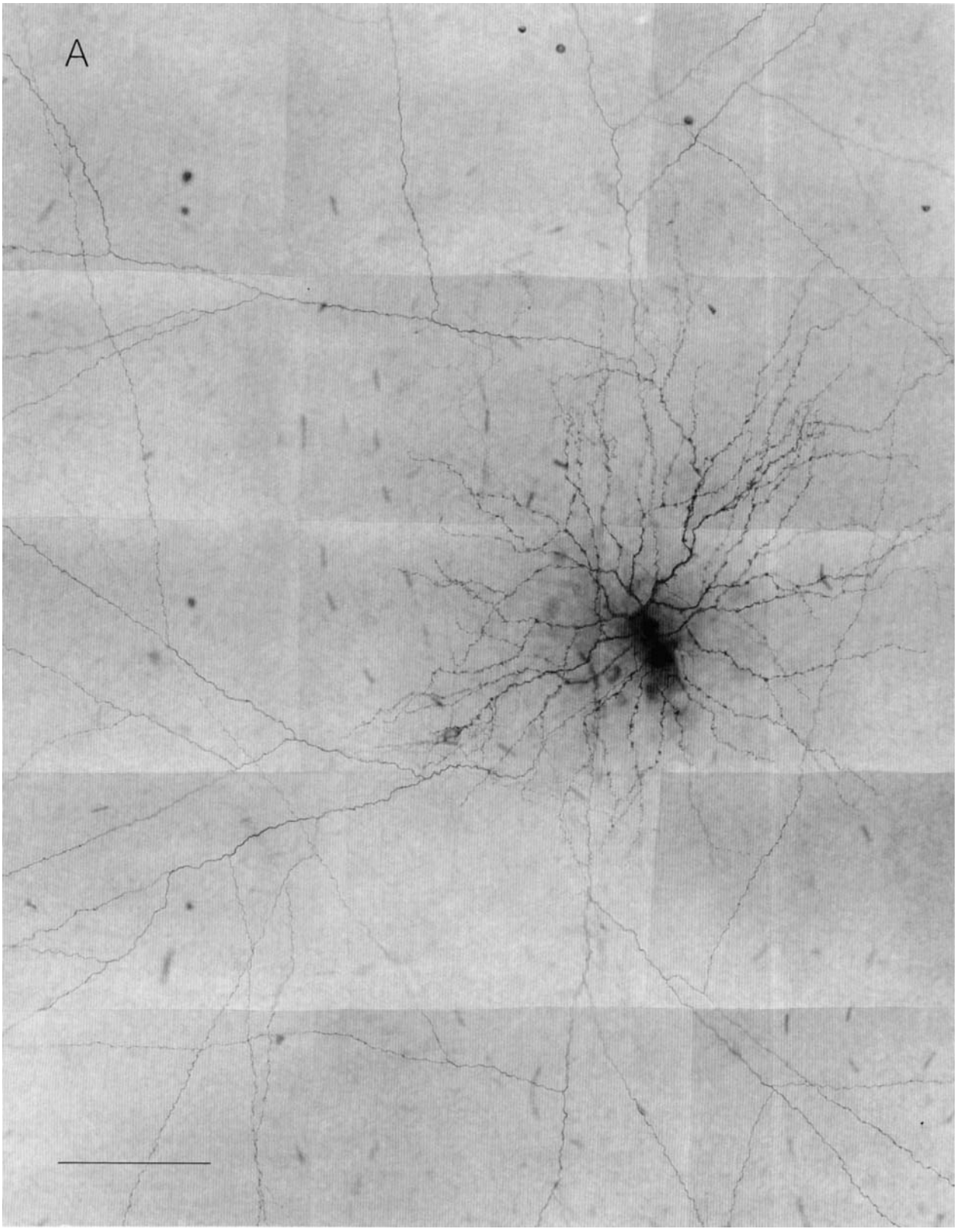

Figure 2

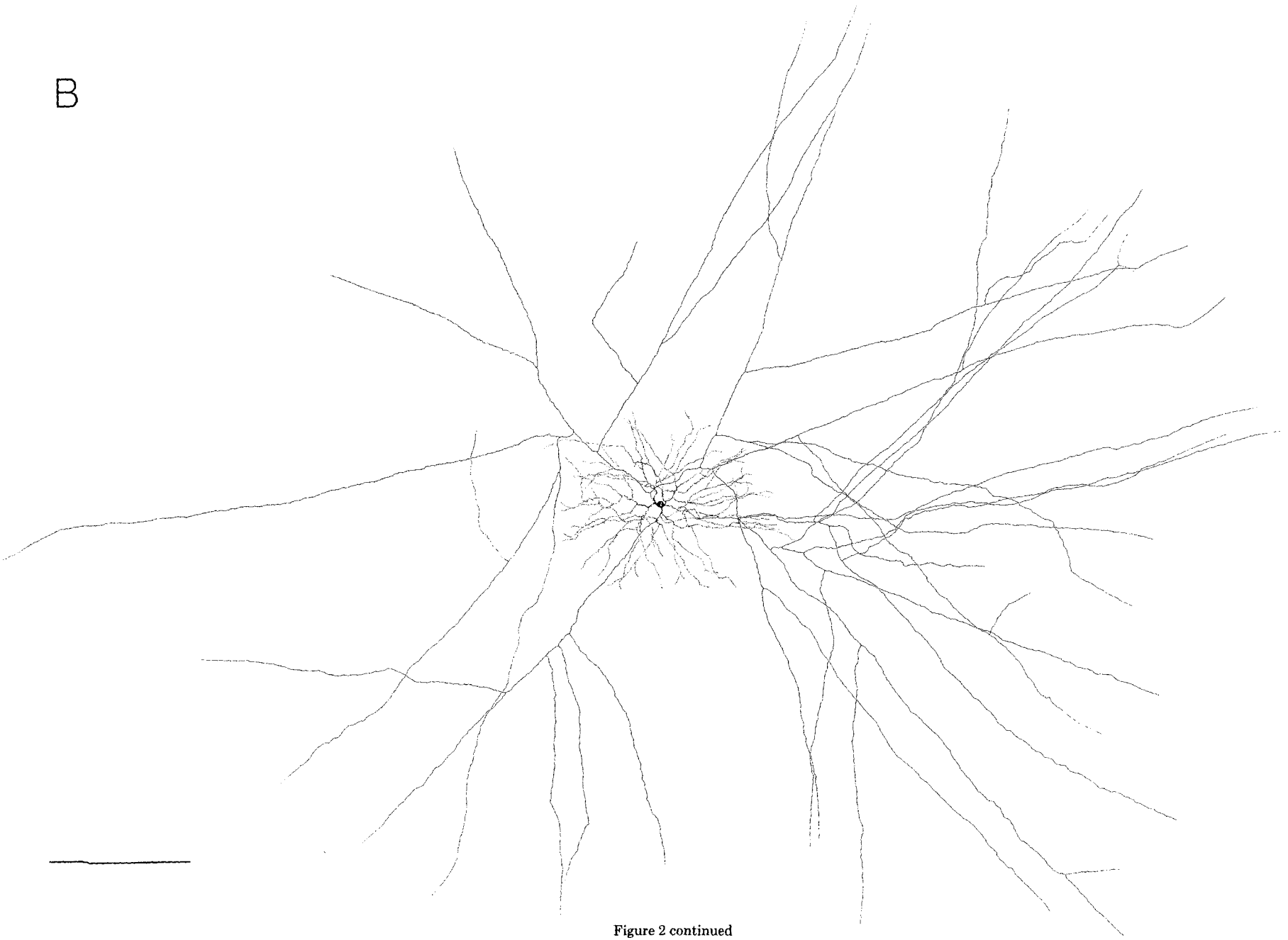

Figure 2 continued

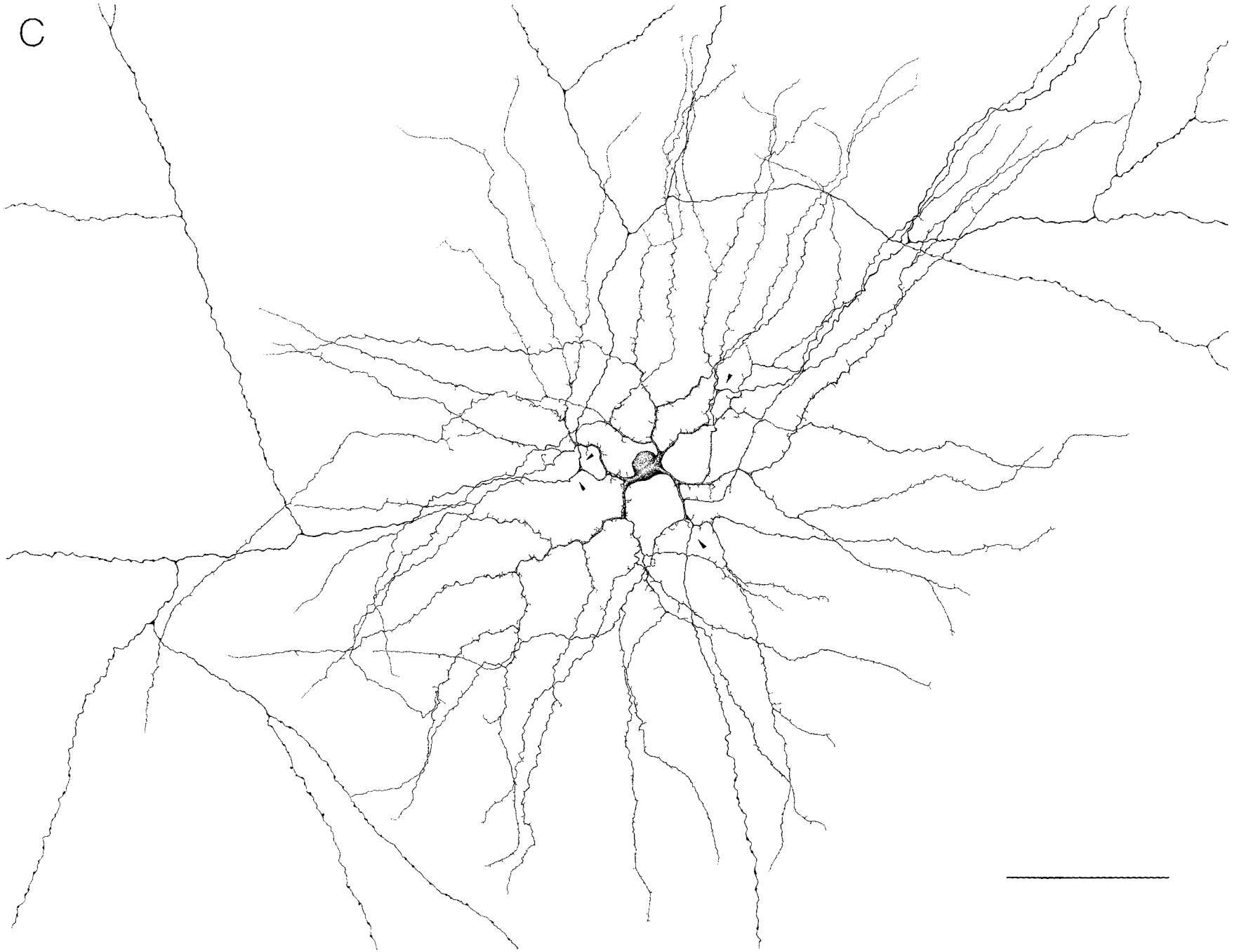

Figure 2 continued

Figure 2 continued

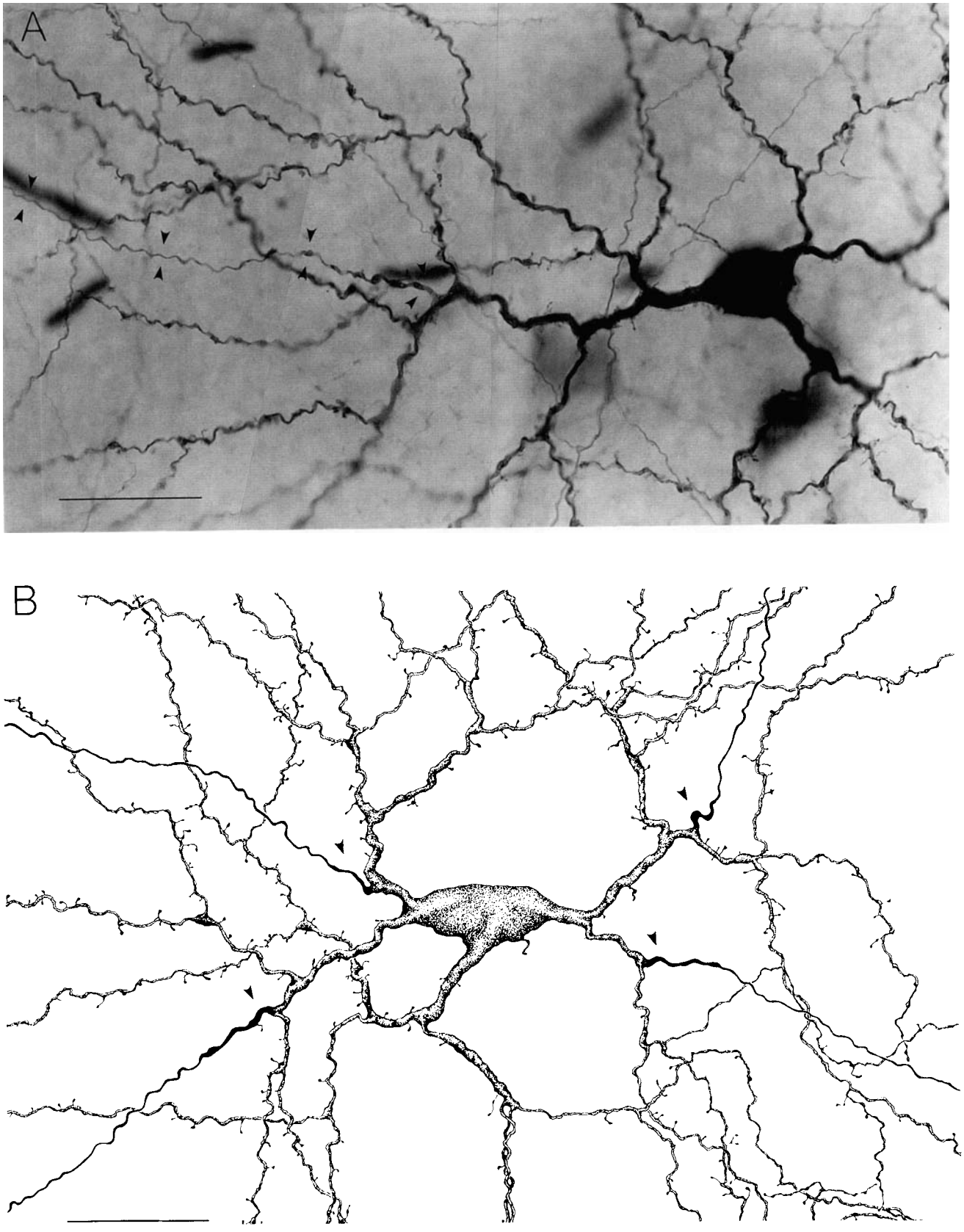

Fig. 3. Proximal dendritic morphology of the axon-bearing amacrine cell of the IPL is illustrated in a photomicrograph (**A**) and a camera lucida tracing (**B**). The large, multipolar soma typically gives rise to three or four thick primary dendrites that radiate in the plane of the soma and bifurcate successively several times. The third- and higher-order branches are long relative to the parent branches and taper along their lengths to become extremely thin (<0.5 μm in diameter). The terminal branches usually extend radially to their termination without further branching but follow an irregular, undulating course through the depth of the IPL (see Fig. 5). The thick proximal dendrites display distinct spinelike processes not obvious on the terminal dendritic branches. The origins of the axons from the dendrites are indicated by the arrowheads in both A and B and are further illustrated in Figure 6. Scale bar in A and B = 25 μm.

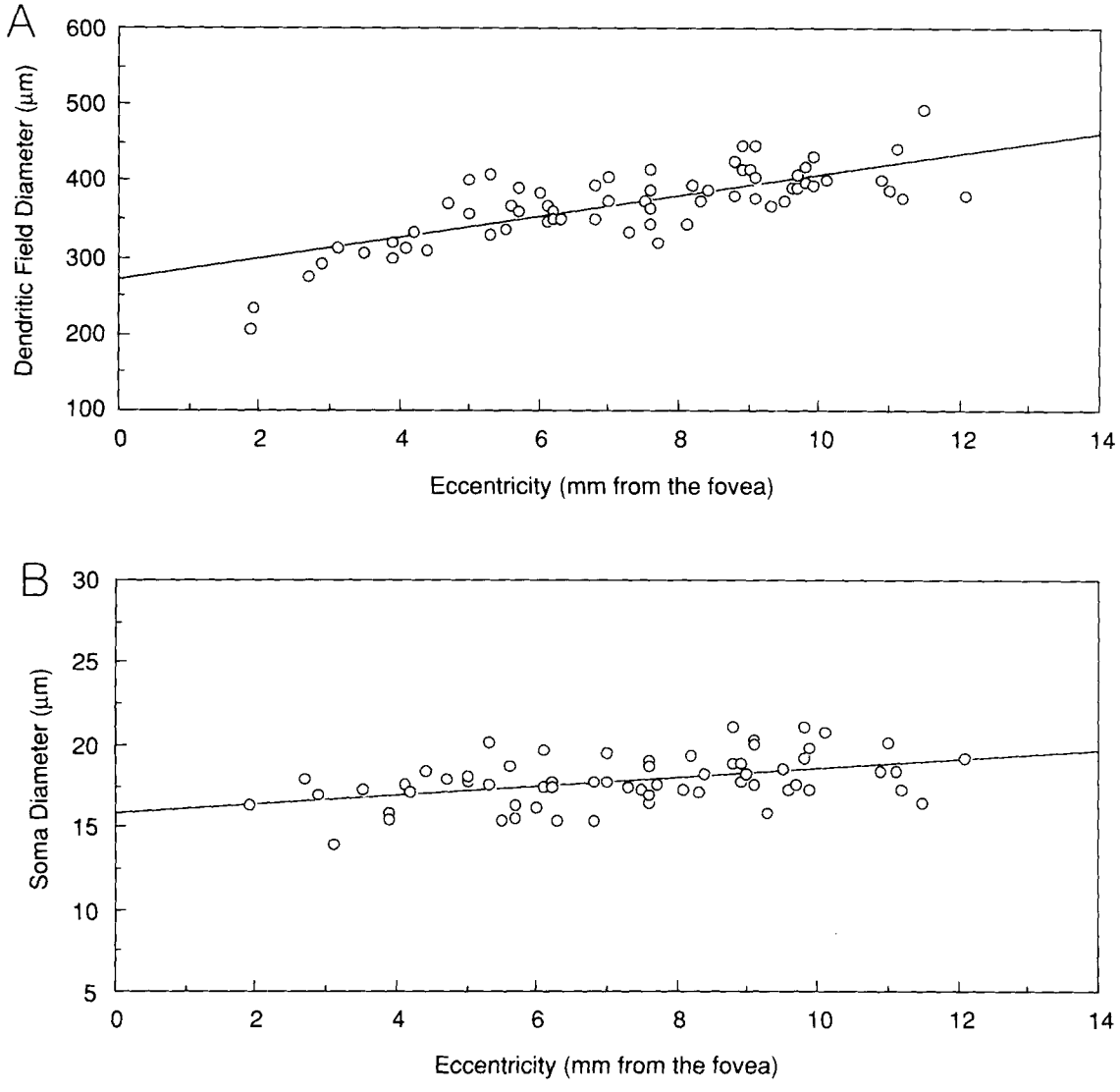

Fig. 4. Dendritic tree and soma size for the axon-bearing amacrines. **A:** Scatter plot of dendritic field diameter as a function of retinal eccentricity for 64 HRP filled axon-bearing amacrine cells shows that the dendritic field size increases from ~200 μm in diameter at 2 mm from the fovea to ~500 μm in the periphery. Linear regression statistics show a positive correlation coefficient of 0.74. **B:** Scatter plot of soma diameter as a function of retinal eccentricity for the same sample of cells shown in A. Diameter ranged from 14 to 21 μm (mean = 17.8 μm, SD = 1.5 μm). Linear regression showed a positive correlation coefficient of 0.45.

cell layers with the IPL. These borders were judged by closing down the microscope condenser diaphragm and bringing the unstained cell bodies at the borders of the two cellular layers into focus. Measurements of IPL thickness made in this way were consistently 11–13 μm (the same measurements made in vitro after acridine staining give an IPL thickness of ~35 μm, indicating a shrinkage of about 70% after mounting and dehydration). The plane of focus of the soma and of the outermost and innermost dendritic branches were measured and expressed as a percentage of the total thickness of the IPL. The stratification of the axonal tree for a single cell was determined by the same method for a number of sampled locations along the axonal branches. The manner in which the dendritic tree occupied the space between the outermost and innermost branches was also determined for a single cell by tracing it with a computer system designed to preserve z-axis depth information during camera lucida tracing (Eutectics) and by using the computer to rotate the cell by 90°.

RESULTS

Identification of axon-bearing amacrine cells in vitro

The axon-bearing amacrine cells could be consistently recognized by the characteristic position of their somata in the IPL. Acridine staining of the retina in vitro produced a bright green fluorescence of somata and nuclei in the ganglion cell layer (GCL) (Fig. 1A) and a less intense fluorescence in the inner nuclear layer (INL). Weakly fluorescing neuronal somata were also observed as the plane of focus

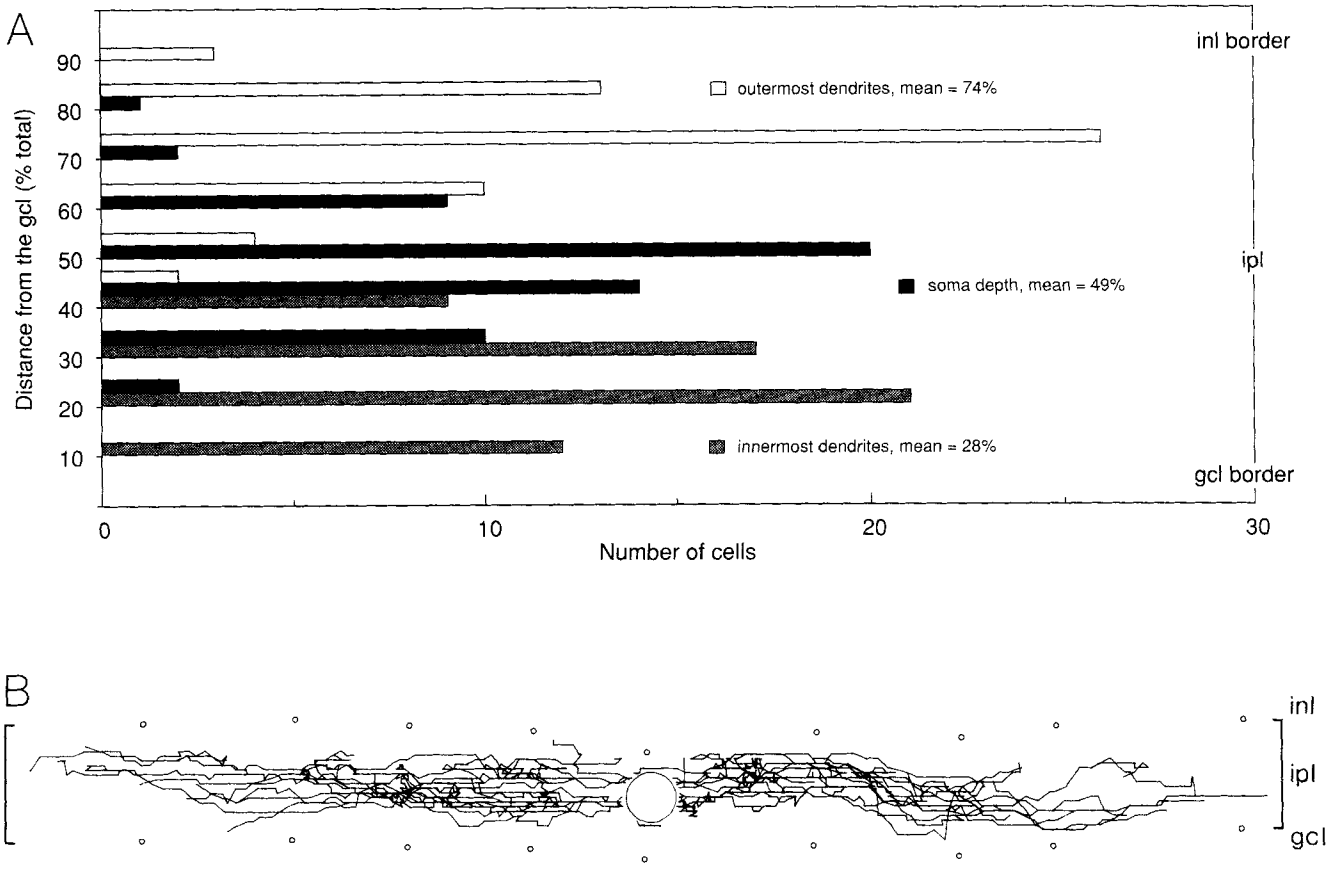

Fig. 5. **A:** Depth of stratification within the IPL for the dendritic tree and soma was determined by measuring the position of the somata and the outermost and innermost borders of the dendritic trees relative to the inner nuclear layer (INL) and ganglion cell layer (GCL) borders for 58 HRP-filled cells. The results are expressed in the histogram as a percentage of the total thickness of the IPL and indicate that the dendritic tree extends over approximately the central 50% of the IPL, bordered by a narrow, unoccupied band along the inner and outer IPL margins. **B:** A 90° computer rotation of the HRP-filled cell illustrated in Figure 9A illustrates the way in which the dendritic tree spans the central portion of the IPL. The dendrites are not segregated but span the entire central portion of the IPL such that soma is situated between the innermost and outermost dendritic branches. The dots on either side of the dendritic tree mark the locations of the GCL and INL borders measured during the initial computer tracing of the cell. Shrinkage along the z-axis, estimated at 70% (see Materials and Methods) was compensated for by the computer before plotting the neuron structure.

was gradually shifted through the IPL (Fig. 1B). Large, round somata (~15–20 μm diameter) were consistently present at a low density in the approximate center of the IPL, 15–20 μm from the borders of both the INL and the GCL when measured in vitro. Intracellular injections of Lucifer Yellow into these cells revealed their dendritic branching pattern and suggested that they composed a morphologically homogeneous group of neurons. Subsequent injections of HRP confirmed this hypothesis and provided a detailed picture of the cell's morphology for analysis. Sixty-four cells have been identified and recovered after HRP injection and provide the data for a light microscopic characterization of the axon-bearing amacrine cells in the following results. Both midget and parasol cells, the most common ganglion cell types of the primate retina (Watanabe et al., '87), and a few other amacrine cell types were occasionally observed in the IPL and injected with HRP. The parasol cells were the only other cells in the IPL that had a soma size and shape that were similar to the axon-bearing amacrines; however, their slightly larger size (~20–25 μm diameter) and tendency to lie closer to the GCL allowed them, with some practice, to be recognized easily.

Well-filled cells recovered after intracellular HRP injection all showed a characteristic and striking dual morphology (Figs. 2, 3): a distinct dendritic tree gave rise to multiple axonlike processes that arborized to form a second, morphologically distinct arbor that concentrically surrounded the dendritic tree. The dendritic tree and axonlike processes were restricted to the IPL, and these neurons were therefore placed in the amacrine cell class. *Axon* was chosen as the best overall light microscopic term to describe the morphology of the long processes. A similar descriptive terminology has evolved for axon-bearing horizontal cell types of the retina (e.g., Mariani, '85). Whether the amacrine cell processes show the ultrastructural features characteristic of functional axons awaits electron microscopic analysis. Evidence for the hypothesis that these processes may actually generate action potentials is considered in the Discussion.

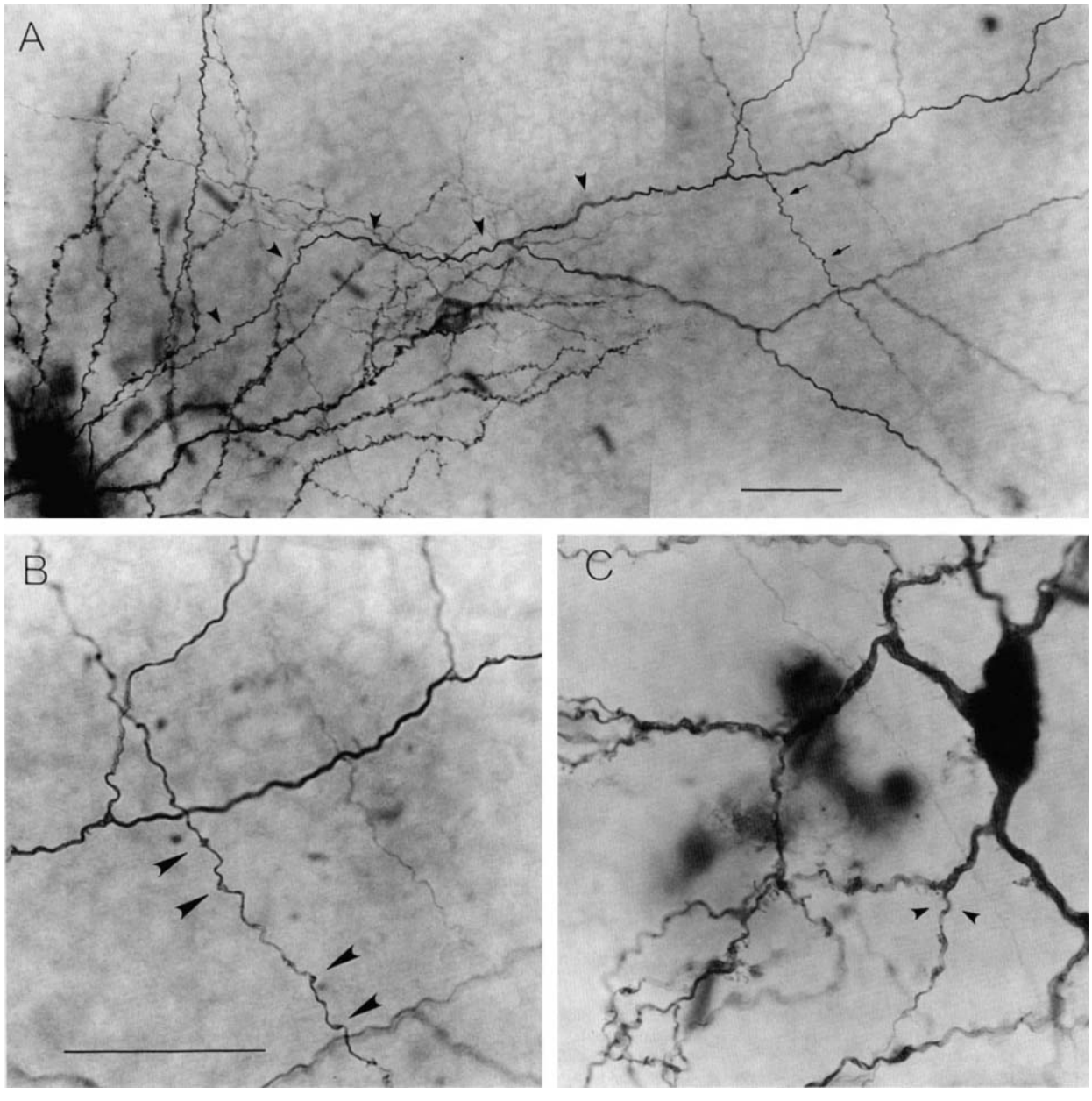

Fig. 6. Axonal morphology of the axon-bearing amacrine cells. From each cell one to four axons (n = 64, mean = 2.5, SD = 0.7) originate close to the soma from the proximal dendrites, typically near the first branch point (mean distance of 29 μm from the soma; SD = 8.9 μm). **A:** At lower magnification this photomicrograph illustrates the initial branching of the axon as it extends beyond the dendritic tree (arrowheads). Note that the axon remains smooth but becomes thicker as it approaches its first branch point. Secondary branches give rise to thin, varicose collaterals (small arrows). **B:** Part of the field in A shown here at higher magnification illustrates the morphological difference between the thick and smooth main branches of the axon and the thinner collateral branches that bear varicosities along their lengths (arrowheads). **C:** The origin of one axon from a proximal dendrite is illustrated by the arrowheads in this photomicrograph (see Fig. 3A for another example). Note that the axon begins as a relatively thick process and then becomes extremely thin and smooth as it courses through the dendritic field. Scale bar for upper and lower panels = 25 μm.

The soma and dendritic tree

A complete camera lucida tracing of a single HRP-filled axon-bearing amacrine cell is illustrated in Figure 2B–D. This cell, located in the temporal retina 9 mm from the fovea, displayed a moderately branched dendritic tree about ~500 μm in diameter. Four thick primary dendrites radiate in the same plane as the soma within the IPL. The primary dendrites branch successively three or four times. The successive branch points tend to occur close to one another, producing a tuft of long terminal dendrites that radiate to

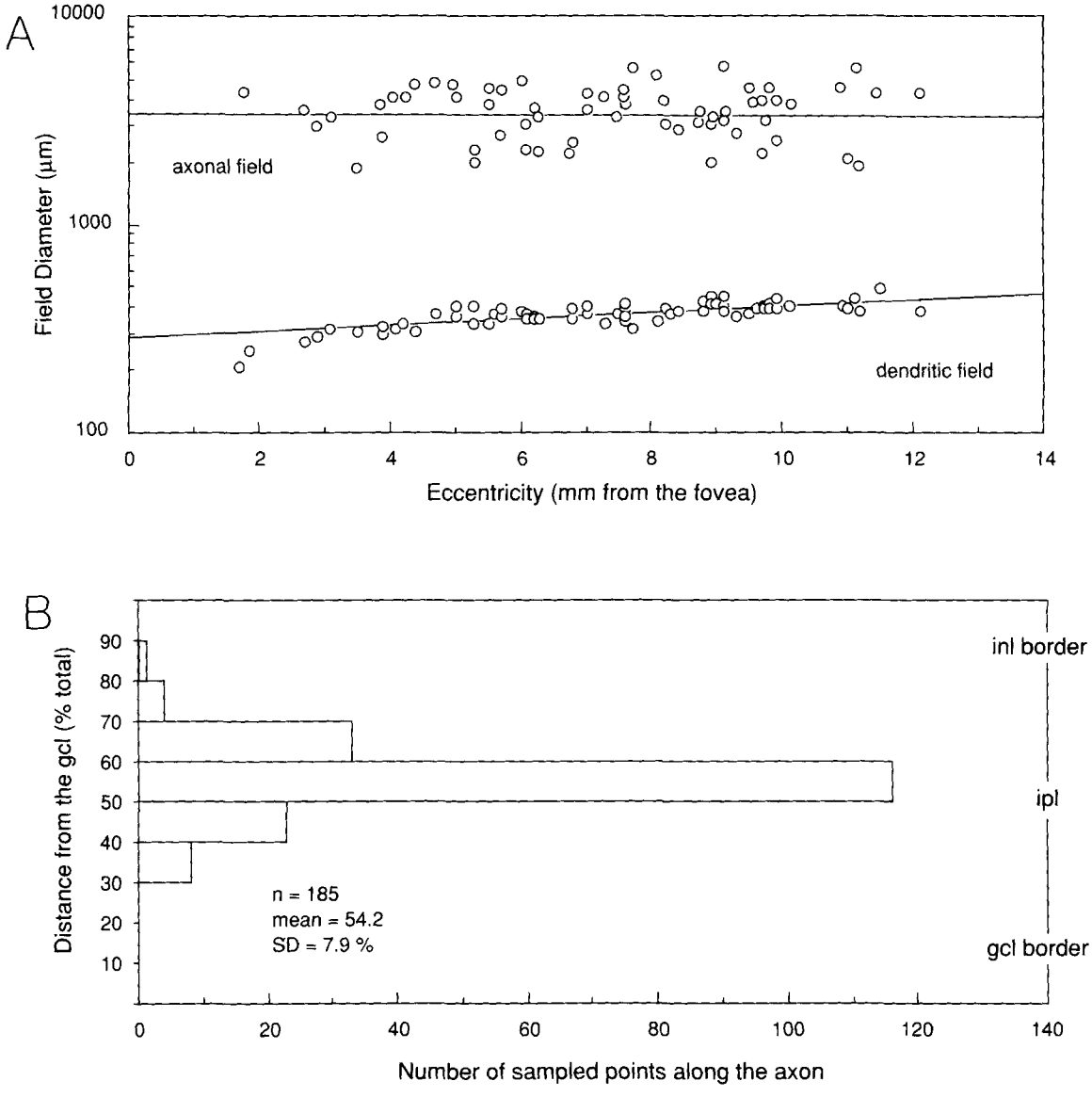

Fig. 7. Size and stratification of the axonal tree. **A:** Scatter plot shows that the estimated diameter of the axonal tree is ~10× that of the dendritic tree. By contrast with the dendritic tree, no increase in axonal tree size with increasing eccentricity was observed. However, this result is tentative because none of the axons were completely revealed by the intracellular HRP injections. **B:** Histogram shows that the axonal tree is located in the approximate center of the IPL but is more narrowly stratified than the dendritic tree. Depth measurements were made at 100 μm intervals along each of the branches of the four axons of the cell illustrated in Figures 5B and 9A. Values were expressed as a percentage of the total depth of the IPL measured at each sample location (see Materials and Methods). The axonal tree was stratified between 40 and 60% of the total depth of the IPL; 137 of a total sample of 185 points fell between these values.

Fig. 8. Estimation of cell density and coverage factor for the axon-bearing amacrine cells. Because it was not possible to do systematic cell counts to determine the density of the axon-bearing amacrine cells, patches of neighboring cells in the IPL were injected with HRP to provide an estimate of local cell density and dendritic coverage factor. **A:**Photomicrograph of two neighboring HRP-filled axon-bearing amacrine cells illustrates the degree of dendritic tree overlap for this amacrine cell population. Scale bar = 200 μm. **B:** Patches of HRP-filled, axon-bearing amacrine cells from central and peripheral retina. The polygons were traced around the extremities of the dendritic branches and the locations of the cell bodies are indicated by the small circle within each polygon. The distance from the fovea is noted adjacent to each patch. The patches suggest that as dendritic tree size decreases centrally cell density increases to maintain a constant coverage factor with changing eccentricity. Cell density for the retinal periphery is estimated at 20–25 cells/mm^2. This density gives an approximate coverage factor of four for the axon-bearing amacrine cells. In striking contrast, the estimated minimum axonal field diameter of 10× that of the dendritic field (Fig. 7) gives a minimum coverage factor for the axonal tree of ~400, or 100× that of the dendritic tree.

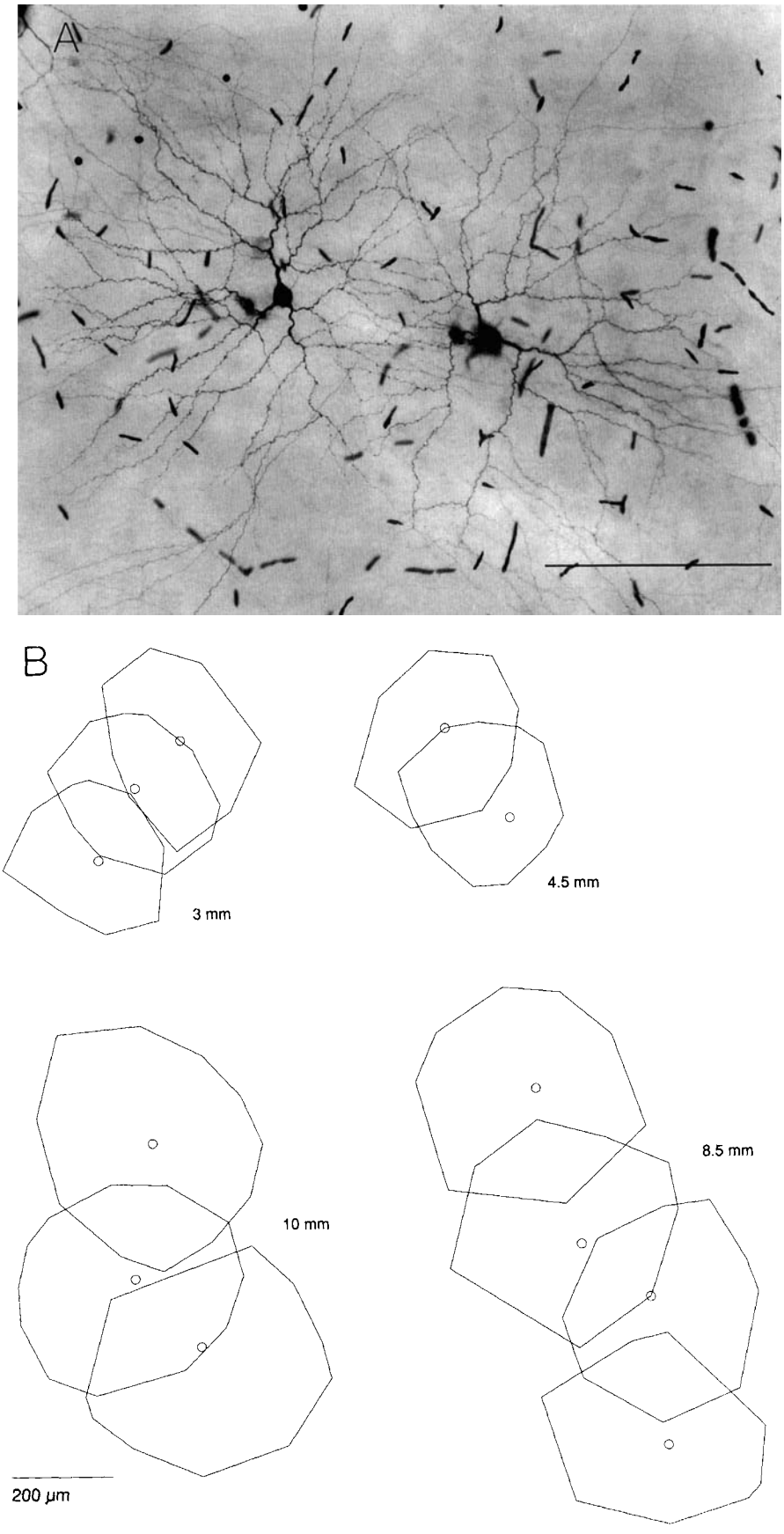

Figure 8

the periphery of the field without much further branching. The dendrites bear a moderate covering of fine spicules, spinelike structures and short, branched appendages (Fig. 3A,B) and can be easily distinguished from the axonal component of the cell, which is considered in detail in the next section.

The relationship of dendritic tree and soma size to distance from the fovea for the axon-bearing amacrines is illustrated in the scatter plots in Figure 4. Dendritic tree size showed a threefold increase, ranging from ~200 μm in diameter (at 1.9 mm from the fovea) to ~600 μm in diameter (at 14 mm eccentricity). This size change showed a strong positive correlation with distance from the fovea (R = 0.74). Soma size ranged from 14 to 21 μm in diameter (n = 64, mean = 17.8 μm, SD = 1.5 μm). A small central-to-peripheral increase in soma size was also present (R = 0.45) (Fig. 4B).

The soma of the axon-bearing amacrine cell was located in the approximate center of the IPL and the dendritic tree appeared broadly stratified such that the soma was situated between the inner and outer dendritic branches. To estimate the stratification of the dendritic tree and soma relative to the total thickness of the IPL, the borders of the INL and GCL, the soma, and the inner and outermost branches of the dendritic tree were brought into focus and their relative depth was read from the calibrated scale on the microscope focus knob for each cell in the sample (Fig. 5A). The results, expressed as % distance from the GCL border, gave a mean depth for the soma of 48% (range = 36–80%, SD = 14%), a mean depth of the innermost dendrites of 28% (range = 18–50%, SD = 10%), and a mean depth for the outermost dendrites of 74% (range = 72–90%, SD = 13%). The manner in which the dendrites were organized over this span of the IPL was determined by making a camera lucida tracing of one cell with a computer system designed to preserve depth information. A 90° computer rotation of this cell (Fig. 5B; a camera lucida tracing of this cell is also illustrated in Fig. 9A) showed that the stratification of the dendritic tree observed in the histogram did not result from the segregation of dendrites at different depths of the IPL; by contrast, individual dendrites followed a wavy course through the entire depth of stratification and frequently crossed over one another. The result is a broadly stratified cell with dendrites that extend over the entire central 50% of the IPL.

The axonal tree

For the majority of cells two or three axons arose from the proximal dendritic tree (n = 64, range = 1–4, mean = 2.5, SD = 0.7). In three instances one axon only was observed, and in one of those cases the axon originated from the soma. There was a clear tendency for the axons to originate from a thick, primary dendrite near the first branch point (Fig. 6). Measurement of the linear distance of the axon's origin from the soma showed a narrow, unimodal distribution (n = 64 cells, mean = 29 μm, range = 12–47 μm, SD = 8.9 μm).

Individual axons showed a characteristic structure that could be reliably distinguished from the cell's dendrites. At their origin on a dendrite the axons often appeared about the same thickness as the parent dendrite; however they immediately tapered to an extremely thin (<0.5 μm), smooth, and straight process that contrasted with the spiny, meandering, and irregularly shaped dendrites (Figs. 3, 6A). As the axon extended beyond the bounds of the dendritic tree it remained smooth but gradually thickened (~1–3 μm). No attempt was made to quantify this distinct thickening, but it was apparent on every axon that was well stained. The axon typically bifurcated once or twice at the border of the dendritic field. These daughter branches coursed in a variety of directions away from the dendritic field and gave rise to fine collateral branches (Figs. 2, 6B). The collaterals bore distinct varicosities along their length and could be traced for 1–3 mm without further branching. The axons that arose from an individual cell radiated away from the cell in different directions such that the total arborization concentrically surrounded the dendritic tree. In instances in which only one or two axons arose from a cell the axons often bifurcated close to their origin, and the daughter branches then radiated in opposite directions to fill in the "open space" in the axonal arbor. Thus despite the variation in axon number (from one to four) the total arborization pattern was essentially the same for each of the cells.

In no instance could an HRP-filled axon be traced to an apparent termination. The DAB reaction product gradually faded, typically at about 2 mm from the soma, until the axon could no longer be clearly observed. Thus to estimate a minimum size for the axonal tree, the longest process on each cell was measured, (n = 64, mean = 1.9 mm, SD = 0.46 mm, range = 0.95–3.2 mm). This process was then taken as the minimum radius of a presumed circular axonal field. A scatter plot of the axonal tree diameter estimated in this way, together with the dendritic tree diameters for the same cells, as a function of retinal eccentricity (Fig. 7A) shows that the axonal tree is at least 10× the size of the dendritic tree in both central and peripheral retina.

The axonal tree was restricted to the IPL and appeared to be stratified in the center of the IPL. To provide a measure of the depth of stratification for the total axonal tree each axon's relative depth was measured at 100 μm intervals along the length of the entire axonal tree of a single cell. At each point the axon's plane of focus relative to the INL and GCL borders was determined as described for the dendritic tree depth (see above). The results for 187 sample points from the four axons of the cell illustrated in Figures 3B and 9A show that the axonal tree is, like the dendritic tree, located in the approximate center of the IPL, but that, by contrast with the dendritic tree, it is more narrowly stratified, spanning the central 20% of the IPL (Fig. 7B).

Estimate of independent axonal and dendritic tree coverage factors

The dendritic field overlap (coverage factor) for the axon-bearing amacrines was estimated by making HRP injections into neighboring axon-bearing amacrine cells in both central and peripheral retina (Fig. 8). Because of the weakness of the acridine fluorescence in the IPL and the contrasting intensity of the overlying cells in the GCL it was not possible to confidently determine cell density by making systematic cell counts. However, in some instances neighboring cells within the IPL were observed and injected. From these examples (Fig. 8A,B) it was possible to make an estimate of cell density from the intercell spacing in the patch of injected cells. In four examples from the retinal periphery injected cell bodies showed a mean near-neighbor separation of 248 μm (n = 16, SD = 44; range = 180–340) giving a density of 20–25 cells/mm^2 assuming an approximate hexagonal packing geometry for the cells (Wässle et al., '81). Multiplying this estimate by dendritic field area for periph-

eral axon bearing amacrine cells gives a coverage factor of four to five. This estimate is consistent with the observed dendritic overlap in the patches and appears to be maintained as cell density increases and dendritic field size decreases in central retina (Fig. 8B).

Given the estimated cell density of 20–25 cells/mm^2 in the retinal periphery and a minimum axonal field diameter of ~6 mm, the coverage factor for the axonal tree would be approximately 500–700, about 100 times that of the dendritic tree. The approximate density of the plexus produced by this extensive overlap can be estimated from the total length of the axonal processes on a single cell. This was found to be ~40 mm for the cell shown in Figure 2. Multiplying this number by cell density gives a total of 800–1,000 mm of axon/mm^2. By contrast, the dendritic tree gives rise to only about 15% of the total length of the cell's processes (~7 mm) and a density of ~150 mm/mm^2. Thus, despite the relatively sparse branching pattern of the axonal tree, the extensive overlap should give rise to a plexus of processes in the IPL at least six times the density of that for the dendritic tree. Given that the axonal tree is not completely filled with HRP and is more narrowly stratified within the IPL than the dendritic tree (Figs. 5, 7) the true density difference is likely to be greater than the above estimate.

DISCUSSION

Several morphological features establish the axon-bearing amacrine as a new and clearly identifiable cell type in the macaque retina. These features include a characteristic dendritic field size, branching pattern, and depth of stratification; the unusual location of the soma in the center of the IPL; and the morphologically distinct axons that originate from the dendritic tree and give rise to a second, widely spreading arborization within the IPL. Although the dual morphology is one of the most striking features of this cell type, its division into distinct dendritic and axonal components is not a unique property of the axon-bearing amacrine identified here. Several Golgi studies have recognized long, axonlike processes that arise from the dendritic trees of amacrine cells in both mammalian and nonmammalian retinas (e.g., Ramón y Cajal, 1893; Famiglietti, '81; Mariani, '82; Kolb et al., '88; Rodieck, '88). Variation in the morphology of the dendrites and axonlike processes of these amacrine cells—from small dendritic trees that give rise to a single axon to large, sparsely branching main dendrites that give rise to multiple axonlike processes—suggests that they include a number of distinct cell types. Several recent studies also reveal multiple axon-bearing amacrine cell types by other anatomical techniques. Somatostatin-immunoreactive amacrine cells of the rabbit's retina show a single axonlike process that arises from the soma and projects for long distances from the inferior to superior retina (Sagar, '87); a similar cell type appears to also be present in the chick's retina (Catsicas et al., '87). Axonlike components have been identified in the morphology of a population of monoamine-accumulating amacrine cells in the cat's retina (Dacey, '86, '88). In these cells each of the main dendrites abruptly tapers to form a thin, bouton-bearing process that extends for ~3 mm beyond the dendritic tree. Neurofibrillar stains in cat and rabbit retina also reveal a single population of wide-field amacrine cells with long, axonlike processes that arise from the distal dendrites, but they appear to be morphologically distinct from the monoamine-accumulating amacrines (Vaney et al., '88). In teleost fish and pond turtle retinas intracellular injections of Lucifer Yellow reveal long, axonlike processes that arise from and extend beyond the dendritic trees of some amacrine cells (Djamgoz et al., '83, '85; Teranishi et al., '87; Ammermüller and Weiler, '88). In these studies the overall extent and detailed morphology of the processes were difficult to determine. However, variation in the responses to light and in the proximal dendritic morphology of the injected cells suggested that a number of morphologically and physiologically distinct cell types were observed.

The recent identification of a second amacrine cell subpopulation in the macaque retina with distinct dendritic and axonal components also indicates the presence of multiple axon-bearing cell types in this species (Dacey, '89). This amacrine cell type corresponds to the large dopaminergic cell type that has been observed with catecholamine histofluorescence (Mariani et al., '84) or immunohistochemical staining for tyrosine hydroxylase (Nguyen-Legros et al., '84). It was identified by its large soma size in acridine-orange-stained retinas maintained in vitro and subsequently recognized as the large dopaminergic amacrine by colocalizing tyrosine hydroxylase immunoreactivity in Lucifer Yellow–injected cells. A comparison of its morphology with the axon-bearing amacrine described in the present study is shown in Figure 9. Although the two cell types display clear dendritic and axonal components the fine morphological details of each component are distinct. The dopaminergic amacrine (Fig. 9B) is easily distinguished by its sparse dendritic branching and dense covering of short, spinelike appendages. Like the axon-bearing amacrine of the IPL the axons of the dopaminergic cell arise from the proximal dendrites very close to the soma and have also been traced for over 3 mm within the IPL. By contrast, the axons on the dopaminergic amacrine are very thin and unbranched in their course through the dendritic field. They lack the thick, smooth primary and secondary branches of the cell shown in Figure 9A and show large varicosities along their entire length. Taken together these observations further support the hypothesis that the axon-bearing amacrines compose a major group of distinct cell types present in the vertebrate retina and that the cell type described in the present results is a single, clearly identified example in the macaque monkey.

What is the function of the axonal component of the axon-bearing amacrine cells? One hypothesis is that the dendritic and axonal components are electrically isolated from one another and have totally independent synaptic functions. This hypothesis predicts that the initial part of the axon would function as a high-resistance path to the passive spread of current between the axon arbor and dendritic tree; both components would then make pre- and postsynaptic contacts and function independently (Nelson et al., '75). However, details of the morphology of the axons argue against this idea. The axons arise close to the soma from thick, axon-hillock-like structures, taper for a short distance, and then gradually flare to a uniform diameter; the main branches give rise to thin terminal collaterals that bear varicosities. All of these features resemble classically recognized axon morphology and suggest the alternative hypothesis that action potentials are triggered at the axon's origin on the proximal dendrites, travel distally, and invade the axonal tree, causing transmitter release from the boutons on the collateral branches.

Figure 9

Caption on page 292

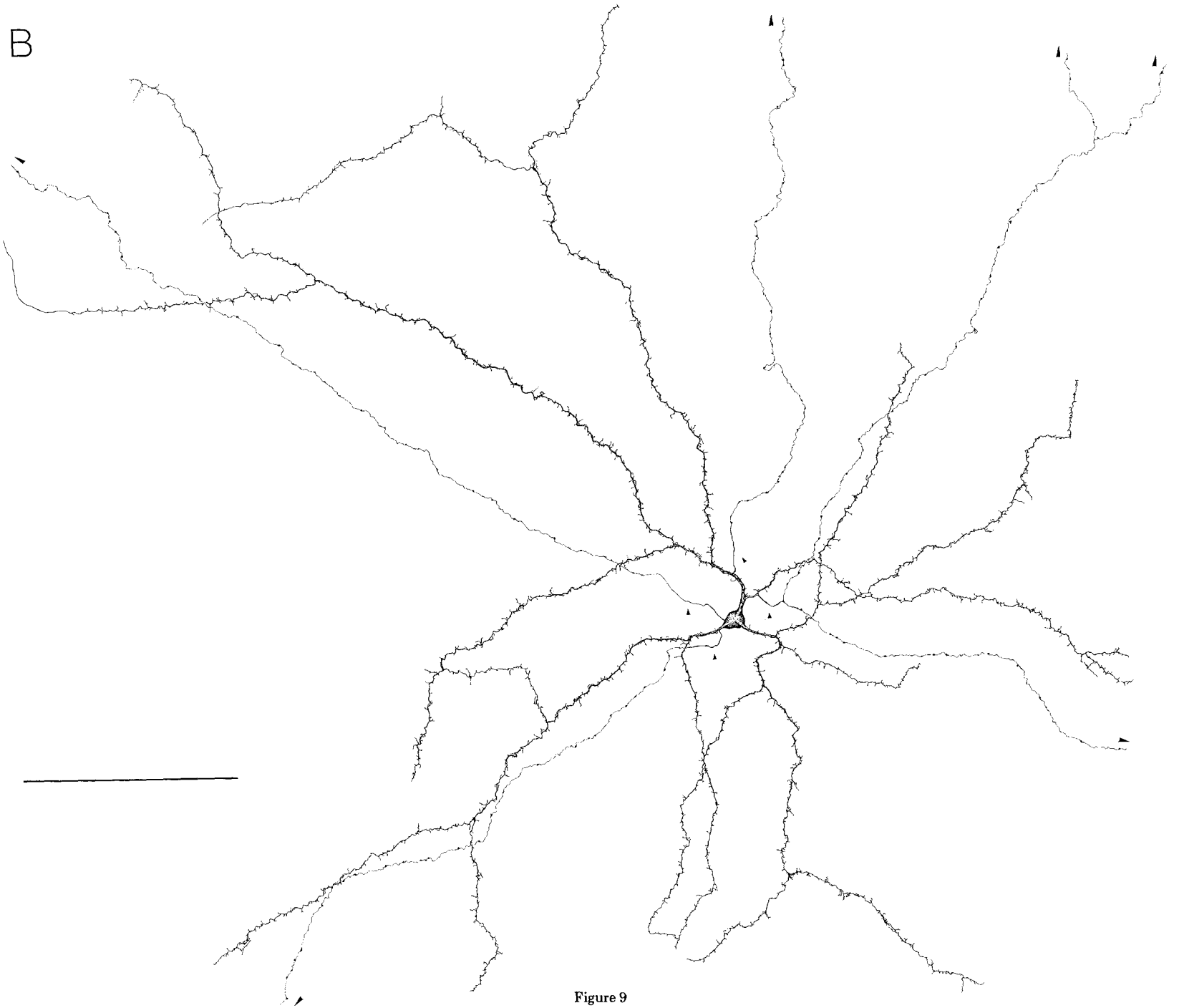

Figure 9

Intracellular recordings from nonmammalian amacrine cells support the spike-generation hypothesis. Tetrodotoxin-sensitive dendritic spikes have been well documented in nonmammalian amacrine cells (Miller and Dacheux, '76; Werblin, '77; Murakami and Shimoda, '77; review, Miller, '79; Barnes and Werblin, '86). Calcium action potentials, have also been described in amacrine cells of the carp's retina (Takahashi and Murakami, '88). Variation in spike size and threshold suggests that the spikes originate from multiple loci at different distances from the recording site. Recently, HRP or Lucifer Yellow injections of teleost amacrine cells after intracellular recording have shown that spiking amacrine cells often give rise to thin, axonlike processes that project beyond the main dendritic tree (Djamgoz et al., '85; Teranishi et al., '87; Ammermüller and Weiler, '88), suggesting a functional link between the axonlike processes and the spikes. Consistent with this possible link, Ammermüller and Weiler ('88) have shown that, for an amacrine cell with distinct dendritic and axonlike components, the receptive field size was relatively small and closely matched to the proximal dendritic tree size, despite the presence of axonlike processes that increased the cell's overall diameter to several millimeters. The axonlike processe thus do not appear to provide a source of inputs to the cell's receptive field center or surround.

If the axons do give rise to spikes that propagate over long distances within the IPL, what might their function be? One clue comes from the mosaic of processes formed by the axon-bearing amacrine subpopulation. The present results show that the extensive overlap of the axonal trees will give rise to a meshwork of processes many times more dense than the axonal tree of a single cell. This meshwork in a given local patch of retina represents convergence of axons that originate from neighboring cells spread concentrically around that patch up to a distance of at least 2–3 mm. Because processes of the axonal tree of a single cell decrease in density with increasing distance from their origin (e.g., Fig. 2B), the synaptic contribution of a single cell to a given local patch would be a weighted function of its distance from that patch. This type of neural geometry could generate a finely graded, local summation of signals that conveys information about the pattern of activity over a relatively large area of visual space (at least 10–15°). Such a neural mechanism is implicated in the ability of ganglion cells to adjust sensitivity to local spatial and temporal changes in contrast beyond the classical receptive field (Werblin, '72; Schwartz, '73; Werblin and Copenhagen, '74; Thibos and Werblin, '78; Enroth-Cugell and Jakiela, '80). This nonlinear behavior has been termed the *contrast gain control* (Shapley and Victor, '79) and, it has been argued, is one of a hierarchy of neural mechanisms subserving visual adaptation (Shapley and Enroth-Cugell, '84).

Is there any evidence for a neurotransmitter candidate for the axon-bearing amacrines of the IPL? GABA immunoreactivity has been observed in large cells located in the middle of the macaque IPL (Hendrickson et al., '85), and several neuropeptides, including substance P, cholecystokinin, corticotropin-releasing factor, and vasointestinal polypeptide, have also been localized in amacrine cell bodies within the IPL (Brecha et al., '82; Tornqvist and Ehinger, '88; D. Marshak, personal communication). The morphology of the peptide-immunoreactive cells suggests, however, that they correspond to other, distinct amacrine cell types (personal observations). By combining Lucifer Yellow injections of axon-bearing amacrine cells with subsequent immunohistochemical demonstration of GABA and other transmitter candidates (e.g., Smithson et al., '84; Werblin et al., '88; Dacey, '89), it should be possible to directly determine the neurotransmitter profile of the axon-bearing amacrines.

Fig. 9. Evidence for multiple types of axon-bearing amacrine cells in the macaque retina: a comparison of the axon-bearing amacrine of the IPL with the dopaminergic amacrine cell. In the Discussion it is argued that the axon-bearing amacrine of the IPL represents only a single example of a number of amacrine cell types in all vertebrate retinas that show axonal and dendritic components. This figure contrasts the morphology of the axon-bearing amacrine cell of the IPL (**A**) with the large dopaminergic amacrine cell (**B**) recently identified in the macaque retina by correlated intracellular injection of Lucifer Yellow and tyrosine hydroxylase immunohistochemistry (Dacey, '89). The dopaminergic amacrine also gives rise to multiple axonlike processes from the cell body or proximal dendrites that may extend beyond the dendritic tree for over 3 mm. However, the two cell types are easily distinguished by clear differences in the detailed morphology and stratification of the both the dendritic and axonal tree. The small arrowheads indicate origins of the axons from the dendritic tree and the large arrowheads in B indicate that the axons have been truncated for the purpose of the illustration. Scale bar = 150 μm in both A and B.

ACKNOWLEDGMENTS

This work was supported by NIH grant EY06678. I thank R.W. Rodieck for a stimulating introduction to the monkey's retina, Helen Sherk for providing the space necessary to carry out this study, and Bill Gardiner for technical assistance. I am also grateful to David Marshak for generously sharing his unpublished immunohistochemical results and to C. Curcio, J.F.M. van Brederode, M. Koontz, and K. Mulligan for carefully reviewing drafts of the manuscript.

LITERATURE CITED

Ames, A., and F.B. Nesbett (1981) In vitro retina as an experimental model of the central nervous system. J. Neurochem. *37*:867–877.

Ammermüller, J., and R. Weiler (1988) Physiological and morphological characterization of OFF-center amacrine cells in the turtle retina. J. Comp. Neurol. *273*:137–148.

Barnes, S., and F. Werblin (1986) Gated currents generate single spike activity in amacrine cells of the tiger salamander. Proc. Natl. Acad. Sci. USA *83*:1509–1512.

Brecha, N. (1983) Retinal neurotransmitters: Histochemical and biochemical studies. In P.C. Emson (ed): Chemical Neuroanatomy. N.Y.: Raven Press, pp. 85–129.

Brecha, N., A. Hendrickson, I. Floren, and H.J. Karten (1982) Localization of substance P-like immunoreactivity within the monkey retina. Invest. Ophthalmol. Vis. Sci. *23*:147–153.

Brown, K.T., and D.G. Flaming (1986) Advanced Micropipette Techniques for Cell Physiology. IBRO Handbook Series, 9: Methods in the Neurosciences. Great Britain: John Wiley & Sons.

Catsicas, S., M. Catsicas, and P.G.H. Clarke (1987) Long-distance intraretinal connections in birds. Nature *326*:186–187.

Dacey, D.M. (1985) Wide-spreading terminal axons in the inner plexiform layer of the cat's retina: Evidence for intrinsic axon collaterals of ganglion cells. J. Comp. Neurol. *242*:247–262.

Dacey, D.M. (1986) Distinct dendritic components of large field amacrine cells in the cat's retina. Soc. Neurosci. Abstr. *12*:199.

Dacey, D.M. (1988) Dopamine-accumulating amacrine cells revealed by in vitro catecholamine-like fluorescence display a unique morphology. Science *240*:1196–1198.

Dacey, D.M. (1989) Distinct dendritic and axonal components of dopaminergic amacrine cells in the macaque monkey retina. Invest. Opthalmol. Vis. Sci. [Suppl.] *30*:319.

Djamgoz, M.B.A., J.E.G. Downing, and H.-J. Wagner (1983) The dendritic fields of functionally identified amacrine cells in a cyprinid fish retina. J. Physiol. (Lond.) *349*:21P.

Djamgoz, M.B.A., J.E.G. Downing, E. Wagner, H.-J. Wagner, and I. Zeutzius (1985) Functional organization of amacrine cells in the teleost fish retina. In A. Gallego and P. Gouras (eds): Neurocircuitry of the Retina, A Cajal Memorial. Amsterdam, The Netherlands: Elsevier Publishing Co. pp. 188–204.

Dowling, J.E., and B.B. Boycott (1966) Organization of the primate retina: Electron microscopy. Proc. R. Soc. Lond. [Biol.] *166*:80–111.

Dowling, J.E. (1968) Synaptic organization of the frog retina: An electron microscopic analysis comparing the retinas of frogs and primates. Proc. R. Soc. Lond. [Biol.] *170*:205–228.

Dowling, J.E. (1987) The Retina: An Approachable Part of the Brain. Cambridge, Mass: Belknap Press.

Elias, S.A., and J.K. Stevens (1980) The dendritic varicosity: A mechanism for electrically isolating the dendrites of cat retinal amacrine cells. Brain Res. *196*:365–372.

Enroth-Cugell, C., and H.G. Jakiela (1980) Suppression of cat retinal ganglion cell responses by moving patterns. J. Physiol. (Lond.) *302*:49–72.

Famiglietti, E.V. (1981) Displaced amacrine cells of the retina. Soc. Neurosci. Abstr. *7*:620.

Hendrickson, A.E., M. Ryan, B. Noble, and J.-Y. Wu (1985) Localization of gamma aminobutyric acid (GABA)-containing neurons in Macaca monkey and human retina. Invest. Ophthalmol Vis. Sci. [Suppl.] *26*:95.

Kolb, H., R. Nelson, and A. Mariani (1981) Amacrine cells, bipolar cells and ganglion cells of the cat retina: A Golgi study. Vision Res. *21*:1081–1114.

Kolb, H., I. Perlman, and R.A. Normann (1988) Neural organization of the retina of the turtle, *Mauremys caspic:* A light microscope and Golgi study. Vis. Neurosci. *1*:47–72.

Mariani, A.P. (1982) Association amacrine cells could mediate directional selectivity in pigeon retina. Nature *298*:654–655.

Mariani, A.P. (1985) Multiaxonal horizontal cells in the retina of the tree shrew, *Tupaia glis*. J. Comp. Neurol. *233*:553–563.

Mariani, A.P., H. Kolb, and R. Nelson (1984) Dopamine-containing amacrine cells of rhesus monkey retina parallel rods in spatial distribution. Brain. Res. *322*:1–7.

Masland, R.H., J.W. Mills, and C. Cassidy (1984) The functions of acetylcholine in the rabbit retina. Proc. R. Soc. Lond. [Biol.] *223*:121–139.

Miller, R.F., and R.F. Dacheux (1976) Dendritic and somatic spikes in mudpuppy amacrine cells: Identification and TTX sensitivity. Brain Res. *104*:157–162.

Miller, R.F. (1979) The neuronal basis of ganglion cell receptive field organization and the physiology of amacrine cells. In F.O. Schmitt and F.G. Worden (eds): The Neurosciences Fourth Study Program. Cambridge, Mass: MIT Press, pp. 227–245.

Miller, R.F., and S.A. Bloomfield (1983) Electroanatomy of a unique amacrine cell in the rabbit retina. Proc. Natl. Acad. Sci. USA *80*:3069–3073.

Murakami, M., and Y. Shimoda (1977) Identification of amacrine and ganglion cells in the carp retina. J. Physiol. (Lond.) *264*:801–818.

Nelson, R., A.V. Lützow, H. Kolb, and P. Gouras (1975) Horizontal cells in the cat retina with independent dendritic systems. Science *189*:137–139.

Nguyen-Legros, J., C. Versaux-Botteri, L.H. Phuc, A. Vigny, and M. Gay (1984) Morphology of primate's dopaminergic amacrine cells as revealed by TH-like immunoreactivity on retinal flatmounts. Brain Res. *295*:145–153.

Ramón y Cajal, S. (1893) La rétine des vertébrés. La Cellule *9*:17–257.

Rodieck, R.W. (1988) The primate retina. In H.D. Steklis and J. Erwin (eds): Comparative Primate Biology, Vol. 4: Neurosciences. New York: Alan R. Liss, Inc., pp. 203–278.

Sagar, S. (1987) Somatostatin-like immunoreactive material in the rabbit retina: Immunohistochemical staining using monoclonal antibodies. J. Comp. Neurol. *266*:291–299.

Sakai, H., K.-I. Naka, and J.E. Dowling (1986) Ganglion cell dendrites are presynaptic in the catfish retina. Nature *319*:495–497.

Sandell, J.H., and R.H. Masland (1986) A system of indoleamine-accumulating neurons in the rabbit retina. J. Neurosci. *6*:3331–3347.

Schwartz, E.A. (1973) Organization of ON-OFF cells in the retina of the turtle. J. Physiol. (Lond.) *230*:1–14.

Shapley, R.M., and C. Enroth-Cugell (1984) Visual adaptation and retinal gain controls. Prog. Retinal Res. *3*:263–346.

Shapley, R.M., and J.D. Victor (1979) The contrast gain control of the cat retina. Vision Res. *19*:431–434.

Smithson, K.G., P. Cobbett, B.A. MacVicar, and G.I. Hatton (1984) A reliable method for immunocytochemical identification of Lucifer Yellow injected peptide-containing mammalian central neurons. J. Neurosci. Methods *10*:59–69.

Takahashi, K.-I., and M. Murakami (1988) Calcium action potential in ON-OFF transient amacrine cells of the carp retina. Brain Res. *456*:29–37.

Tauchi, M., and R.H. Masland (1984) The shape and arrangement of the cholinergic neurons in the rabbit retina. Proc. R. Soc. Lond. [Biol.] *223*:101–119.

Tauchi, M., and R.H. Masland (1986) Subpopulations of catecholaminergic neurons in the rabbit retina. Soc. Neurosci. Abstr. *12*:198.

Teranishi, T., K. Negishi, and S. Kato (1987) Functional and morphological correlates of amacrine cells in carp retina. Neuroscience *20*:935–950.

Thibos, L., and F.S. Werblin (1978) The properties of surround antagonism elicited by spinning windmill patterns in the mudpuppy retina. J. Physiol. (Lond.) *278*:101–116.

Tornqvist, K., and B. Ehinger (1988) Peptide immunoreactive neurons in the human retina. Invest. Ophthalmol Vis. Sci. *29*:680–686.

Vaney, D.I. (1985) The morphology and topographic distribution of AII amacrine cells in the cat retina. Proc. R. Soc. Lond. [Biol.] *224*:475–488.

Vaney, D.I. (1986) Morphological identification of serotonin-accumulating neurons in the living retina. Science *233*:444–446.

Vaney, D.I., L. Peichl, and B.B. Boycott (1988) Neurofibrillar long range amacrine cells in mammalian retinae. Proc. R. Soc. Lond. [Biol.] *235*:203–219.

Voigt, T., and H. Wässle (1987) Dopaminergic innervation of AII amacrine cells in mammalian retina. J. Neurosci. *12*:4115–4128.

Wässle, H., L. Peichl, and B.B. Boycott (1981) Dendritic territories of cat retinal ganglion cells. Nature *292*:344–345.

Wässle, H., T. Voigt, and B. Patel (1987) Morphological and immunocytochemical identification of indolamine-accumulating neurons in the cat retina. J. Neurosci. *7*:1574–1585.

Watanabe, M., R.W. Rodieck, and D.M. Dacey (1987) Parasol ganglion cells of the macaque and baboon retinas. Invest. Ophthalmol. Vis. Sci. *28*:261.

Werblin, F.S. (1972) Lateral interactions at the inner plexiform layer of vertebrate retina: Antagonistic responses to change. Science *175*:1008–1010.

Werblin, F.S. (1977) Regenerative amacrine cell depolarization and formation of on-off ganglion cell response. J. Physiol. (Lond.) *264*:767–785.

Werblin, F.S., and D.R. Copenhagen (1974) Control of retinal sensitivity. III. Lateral interactions at the inner plexiform layer. J. Gen. Physiol. *63*:88–101.

Werblin, F., S. Wu, G. Maguire, and P. Lucasiewicz (1988) Double Lucifer Yellow and anti-GABA staining reveals that narrow field amacrine cells are GABAergic in the tiger salamander retina. Invest. Ophthalmol. Vis. Sci. *29*:103.